Transition from parabolic to ring-shaped valence band maximum in few-layer GaS, GaSe, and InSe

Dmitry V. Rybkovskiy,[1,*] Alexander V. Osadchy,[1,2] and Elena D. Obraztsova[1,2]

[1]*A. M. Prokhorov General Physics Institute, Russian Academy of Sciences, 38 Vavilov Street, 119991 Moscow, Russia*

[2]*National Research Nuclear University MEPhI (Moscow Engineering Physics Institute), 31 Kashirskoye Shosse, 115409 Moscow, Russia*

(Received 19 September 2014; revised manuscript received 5 November 2014; published 1 December 2014)

By performing first-principles electronic structure calculations in frames of density functional theory we study the dependence of the valence band shape on the thickness of few-layer III-VI crystals (GaS, GaSe, and InSe). We estimate the critical thickness of transition from the bulklike parabolic to the ring-shaped valence band. Direct supercell calculations show that the ring-shaped extremum of the valence band appears in β-GaS and β-GaSe at a thickness below 6 tetralayers (∼4.6 nm) and 8 tetralayers (∼6.4 nm), respectively. Zone-folding calculations estimate the β-InSe critical thickness to be equal to 28 tetralayers (∼24.0 nm). The origin of the ring-shaped valence band maximum can be understood in terms of $\boldsymbol{k}\cdot\boldsymbol{p}$ theory, which provides a link between the curvature of the energy bands and the distance between them. We explain the dependence of the band shape on the thickness, as well as the transition between two types of extremes, by the $\boldsymbol{k}$-dependent orbital composition of the topmost valence band. We show that in the vicinity of critical thickness the effective mass of holes in III-VI compounds depends strongly on the number of tetralayers.

DOI: 10.1103/PhysRevB.90.235302 PACS number(s): 31.15.A−, 73.50.Gr, 73.22.−f

I. INTRODUCTION

The III-VI group semiconducting layer compounds GaS, GaSe, and InSe were discovered in the 1930s [1–3] but attracted considerable attention only in the 1950s–1980s due to their strong structural anisotropy [4–8] and remarkable nonlinear optical properties [9–18]. Each layer of these materials has a hexagonal symmetry and is composed of two planes of metal atoms, sandwiched between two chalcogen planes. The bonds inside such a tetralayer are of covalent type with some ionic contributions [19,20]. The layers are stacked together with predominantly van der Waals forces and the stacking geometry determines the polytype of macroscopic crystal [21]. The simplest and most frequently described polytypes are β, ϵ, and γ. The crystal structure of the most symmetric, β modification, is presented in Fig. 1.

Since the successful fabrication of graphene [22], the layered materials have become an object of intense research due to the possibility of obtaining 2D crystals with a thickness of several atoms. Recently, single tetralayers of GaS and GaSe have been fabricated using a mechanical exfoliation method and characterized with atomic force microscopy and Raman scattering spectroscopy [23]. Photodetectors, based on ultrathin GaSe, show a fast response, a high responsivity, and a high quantum efficiency [24].

The applicability of nanomaterials in electronic and optoelectronic devices is determined by their electronic structure. The energy bands of single tetralayers of various III-VI compounds were obtained in the 1960s and 1970s by different authors [25–30]. These computations were based on semiempirical approaches with the aim to investigate the electronic properties of bulk compounds within the so-called 2D approximation, the use of which was determined by the lack of computational resources needed for a full-scale computation of macroscopic III-VI semiconductors. For a realistic and accurate description of electronic energy bands of few-layer GaS, GaSe, and InSe, first-principles computations are needed.

In our previous studies we investigated the quantum confinement effects related to the reduction of GaSe crystal thickness by means of density functional theory (DFT) within the local density approximation [31,32]. Besides a large increase of the quasiparticle gap, we found a qualitative change of the topmost valence band. While the valence band maximum is located at Brillouin zone center in the bulk, it is shifted towards K point in a single tetralayer. Recently it was found that the valence band maximum (VBM) has a sombrero hat shape [33]. A similar feature was previously found to exist in bulk InSe under pressure [34–36]. The authors found an increase of concentration and mobility of holes, associated with the formation of a ring-shaped VBM under pressure above 4 GPa.

In the present work we investigate the evolution of VBM in few-layer GaS, GaSe, and InSe and determine the critical thickness, at which the transition from the parabolic to ring-shaped VBM occurs.

II. COMPUTATIONAL METHODS

To investigate the dependence of the electronic valence band structure on the thickness of GaS, GaSe, and InSe compounds, we performed first-principles calculations based on a plane wave pseudopotential density functional theory. Since the experimental data on the ultrathin III-VI sheets is very limited, to determine the most adequate theoretical approximation we calculated the equilibrium geometry and electronic band structures of bulk β-polytype GaS, GaSe, and InSe crystals using the different types of pseudopotentials and various exchange-correlation functionals.

We found that the use of the PBE [37] functional leads to the overestimation of intralayer bond lengths and cannot reproduce the interlayer bonding, thus leading to a wrong c lattice parameter. The use of the PBEsol [38] functional gave improved in-plane interatomic distances, though the interlayer separation was still overestimated compared to experiment.

*RybkovskiyD@gmail.com

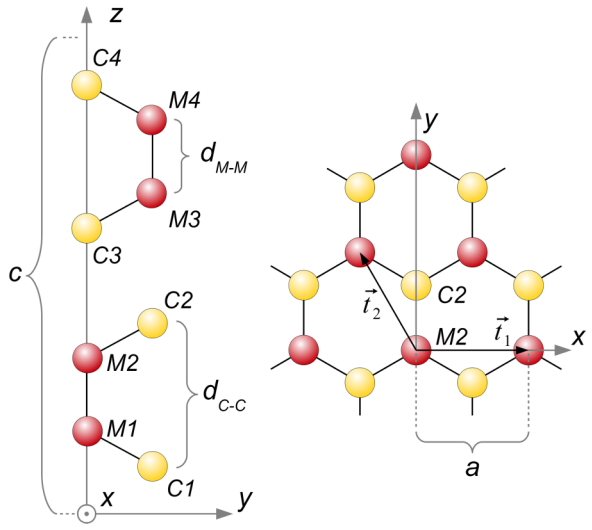

FIG. 1. (Color online) The atomic structure of β modification of the III-VI compound family. The chalcogen (S/Se) and metal (Ga/In) atoms are marked as C and M, respectively.

This is a consequence of the fact that the interlayer coupling is mostly driven by van der Waals interactions, which are not reproduced by the PBE and PBEsol energy functionals. To overcome this problem, we employed the DFT-D2 [39,40] method with the PBE functional to include semiempirical corrections to the total energy. We found that this approach leads to the best agreement between the calculated and experimentally measured crystal geometry of bulk III-VI crystals. However, we discovered that the use of the PBE-D method in the case of single-tetralayer structures leads to an unexpected order change of the topmost valence bands in single-layer InSe. Therefore we performed our final calculations using a simpler LDA functional that, due to its overbinding tendency, allowed us to mimic the attractive interlayer interaction and, thus, allowed us to reproduce a binding between tetralayers. The overall lattice constants and interatomic distances obtained within LDA are given in Table I.

We also noticed that the inclusion of spin-orbit coupling (SOC) is crucial for a fair reproduction of the in-plane hole effective masses of III-VI materials. For instance, in case of β-GaSe, the value of $m_\perp$, calculated without the spin-orbit coupling at theoretical equilibrium lattice geometry, was equal to $1.4m_0$ (as compared with the experimental $0.8m_0$). The inclusion of spin-orbit coupling resulted in a value of $m_\perp =$ $1.0m_0$ (in a better agreement with experiment). At the same time we found that the optimized lattice geometry is weakly affected by a spin-orbit coupling. We therefore performed the structural relaxation without taking the SOC into account to save the calculation time, but we included it in the band structure computations.

TABLE I. The calculated lattice parameters of bulk β-GaS, β-GaSe, and β-InSe, together with the experimental values, taken from literature (in angstroms).

	GaS		GaSe		InSe	
	LDA	Ref. [41]	LDA	Ref. [42]	LDA	Ref. [37]
a	3.54	3.587	3.72	3.755	3.97	4.00
c	15.23	15.49	15.74	15.94	16.45	16.88
$d_{M\text{-}M}$	2.41	2.45	2.41	2.46	2.74	2.80
$d_{C\text{-}C}$	4.57	4.60	4.74	4.78	5.29	5.37

All calculations have been performed using the QUANTUM ESPRESSO code [43]. The action of core electrons was modeled by the use of scalar relativistic and full relativistic ultrasoft pseudopotentials. The $3d$ electrons of Ga/In have been considered as valence electrons. The wave functions have been expanded into a plane wave basis set with the energy cutoff of 80 Rydberg. The cutoff for the charge density and potential was equal to 480 Ry. For the Brillouin zone sampling of the bulk material we used a $12 \times 12 \times 4$ $\boldsymbol{k}$-point grid. For calculations of few-layer structures the supercell method was used with a distance between the surfaces of periodically repeated images of 20 Å. A $12 \times 12 \times 1$ $\boldsymbol{k}$-point grid was used in the case of two-dimensional structures.

To determine the equilibrium crystal geometry the BFGS algorithm was employed. The geometry optimization in each case has been carried out in two steps. First, only the ion positions have been allowed to relax until all components of all forces acting on atoms became smaller than 10^{-4} Ry/a.u. and until the total energy changed less than $10^{-6}N$ Ry, where N is the number of tetralayers in the system. Next, both ions and cell parameters were optimized until the pressure became less than 0.5 kbar.

III. RESULTS AND DISCUSSION

A. Valence bands of III-VI single tetralayers

The optimized lattice constants of single-tetralayer GaS, GaSe, and InSe were found to be 0.2%–0.4% less than in case of bulk materials. After the structural relaxation, the electronic energy bands of these materials have been calculated. The resulting dispersion relations, plotted along the high-symmetry directions of the two-dimensional hexagonal Brillouin zone, are shown in Fig. 2. The energy curves of the conduction bands are gray colored, since LDA is known to be inaccurate in reproduction of the excited-state energies. The zero energy is adjusted to the top of the valence band.

The nature of the valence electron states of the III-VI compounds has been studied many times [19,26], so we give only a short overview. The lowest group of narrow bands is formed by $3d$ orbitals of In/Ga atoms. Their small width is a consequence of a weak special overlap between the corresponding wave functions. The next two energy bands correspond to the S/Se s orbitals. They are considerably separated from the higher electronic bands. The energy states, lying in the range of -7 to 0 eV, are of the most interest due to their strong hybridization and proximity to the valence zone top. We will focus on the uppermost curves, which might participate in optical and transport properties. The topmost valence band at Γ is formed by S/Se p_z orbitals and Ga/In s orbitals. Just below them one can see 8 close-lying energy states, partially split by spin-orbit coupling. At Γ point they consist of p_x and p_y orbitals of S/Se.

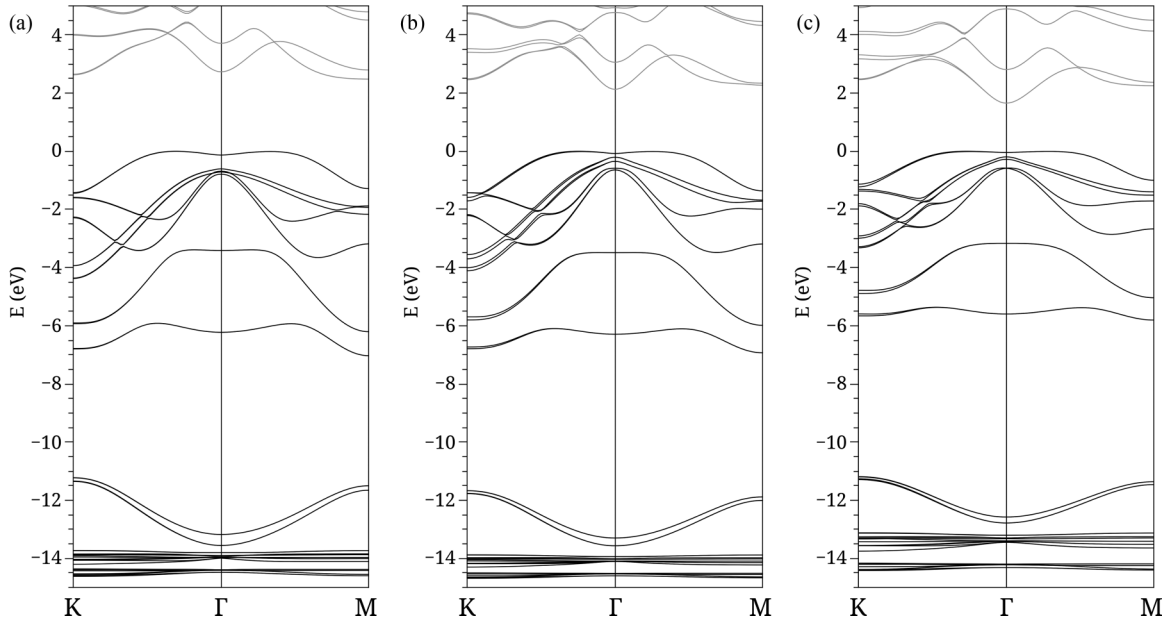

FIG. 2. The electronic energy band structures of single tetralayers of (a) GaS, (b) GaSe, and (c) InSe calculated within LDA with the spin-orbit coupling effects taken into account.

The most striking difference between the valence band structure of III-VI single tetralayers and their bulk counterparts is the shape of the topmost valence band. Unlike in the bulk case, where the valence band maximum is located in the Brillouin zone center, in the single-tetralayer material the corresponding energy curve has a local minimum at this point. The maximum is shifted along the Γ-K direction towards K. The local maximum at the Γ-M direction lies a few meV below the global one. We find that this behavior is similar to that observed in a bulk InSe under pressure [34]. Segura and co-workers found a great increase of the hole concentration and mobility in InSe under pressure above 4 GPa. This finding was related to the emergence of a new ring-shaped valence band maximum (RSVBM). They have also shown that the density of states (DOS) of this kind of extremum has a 2D energy dependence, rather than a 3D one, common for parabolic bands in macroscopic materials. The origin of a ring-shaped maximum was explained on the basis of $\boldsymbol{k}\cdot\boldsymbol{p}$ theory. It is possible to draw a similar picture for case of a single III-VI tetralayer.

The $\boldsymbol{k}\cdot\boldsymbol{p}$ theory allows us to link the curvature (or effective mass) of energy bands with the distance between them. In the case of a nondegenerate level E_n an inverse of the effective mass m_n^* at $k = k_0$ is given by

$$\frac{m_0}{m_n^*} = 1 + \frac{2}{m_0}\sum_{j\neq n}\frac{|\mathbf{p_{nj}}|^2}{E_n(\mathbf{k_0}) - E_j(\mathbf{k_0})}, \qquad (1)$$

where m_0 is a free-electron mass and $\mathbf{p}_{nj}$ are the momentum matrix elements between the states n and j. The interaction of band n with the underlying bands ($E_j < E_n$) tends to decrease the effective mass m_n^*, while interaction with the higher bands ($E_j > E_n$) tends to increase it. Moreover, it can be seen from Eq. (1) that the closer the band j is, its contribution to the effective mass of band n is more substantial. In the case of the topmost valence band of a single-tetralayer III-VI, the closest states are the lower-lying valence bands, formed by p_x and p_y S/Se orbitals, and the higher conduction band. The selection rules for the interaction between these states are contained inside $\mathbf{p}_{nj}$, and can be derived from group theory. We will drop the spin-orbit coupling effects, as they do not affect the qualitative picture. The topmost valence band at Γ transforms according to the Γ_1^+ representation of group D_{3h}^1. For the in-plane hole effective mass $m_\perp$, the interaction is allowed with the lower state with Γ_3^+ symmetry, while there is no coupling with the bottom of the conduction band Γ_2^- due to a vanishing momentum matrix element (Fig. 3). Therefore, the interaction with the nearby state results in a positive curvature of the valence band near the Γ point (as the hole effective mass is opposite to that of electron, this hole mass becomes

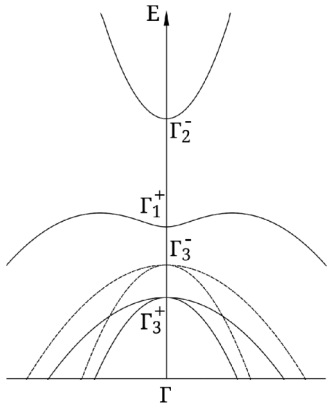

FIG. 3. A sketch of the III-VI single tetralayer electronic bands near the gap, omitting the spin-orbit coupling. In the Brillouin zone center the topmost valence band Γ_1^+ interacts with the underlying Γ_3^+ band, while the coupling with the higher Γ_2^- band is forbidden by symmetry. This results in a local minimum of the dispersion in the zone center.

negative), which leads to an occurrence of a local minimum at the Brillouin zone center. However, when we move away from the Γ point, the topmost valence band is turning downwards. At the point where the dispersion bends, a maximum of the ring-shaped band occurs. In the case of a bulk crystal, the energy separation of states, originated from Γ_1^+ and Γ_3^+, is larger, and the effect of downward dispersion dominates the valence band curvature leading to the large (but positive) hole masses.

To analyze the density of states of the ring-shaped feature, we use an approximate dispersion for the valence band, similar to that proposed by Errandonea *et al.* [35]:

$$E_v(\mathbf{k}) = E_{rs} - \frac{\hbar^2(|\mathbf{k}| - k_{rs})^2}{2m_{rs}}. \quad (2)$$

Here, E_{rs} is the energy of RSVBM, k_{rs} is its radius, and m_{rs} is the parameter controlling the dispersion curvature in the extremum vicinity in the radial direction. In the energy range $E_{rs} \leqslant E_v \leqslant E_{rs} - \hbar^2 k_{rs}^2/2m_{rs}$, the expression for the density of states has the form

$$N(E_v) = E_{rs} - \frac{k_{rs}}{\pi\hbar}\sqrt{\frac{2m_{rs}}{E_{rs} - E_v}}. \quad (3)$$

Different from a two-dimensional parabolic band, where DOS is energy independent, the DOS for a band with a two-dimensional ring-shaped extremum behaves like that of a one-dimensional parabolic band. We calculate the DOS for GaS, GaSe, and InSe single tetralayers within LDA with a tetrahedron method on a $46 \times 46 \times 1$ $\boldsymbol{k}$-point grid with a total of 1060 $\boldsymbol{k}$ points. The resulting plots are presented in Fig. 4. On the zero energy we indeed have found a sharp Van Hove singularity, common for 1D structures. It can be compared with the small, almost energy-independent feature in InSe DOS at 1.67–2.26 eV, arising from the parabolic 2D conduction band. We can therefore conclude that single tetralayers of GaS, GaSe, and InSe have a high, 1D-like electronic density of states of the valence band near the band edge.

A more detailed study of the band shape near the extremum revealed a "warped" rather than ring-shaped behavior, with six global maxima along Γ-K directions and saddle points along the Γ-M direction [33]. In this more refined picture, the sharp peak lying only a few meV below the global maxima in DOS is associated with the presence of these saddle points. For an approximate reproduction of the band shape we modified the model dispersion (2) to take into account the angular dependence of E_v and the nonsymmetric behavior of the electronic band in the vicinity of the global maximum (in polar coordinates):

$$E_v(k,\theta) = A - k^2[B + C\cos(6\theta)] + \sqrt{k^2D^2 + E^2}. \quad (4)$$

Expression (4) is written in atomic units (the resulting energy is, thus, in Hartree units). A, B, C, D, and E are adjustable parameters used to fit the function to the numerical energy band. The model dispersion was fitted in an area of $\boldsymbol{k}$ space with the radius of 0.3 rad/bohr from the Brillouin zone center. The values of A, B, C, D, and E for the single-tetralayer structures are given in Table II.

A comparison of the numerical DFT valence band surface of a single GaS tetralayer with the results obtained with the use of a model dispersion (4) with parameters from Table II is given in Fig. 5.

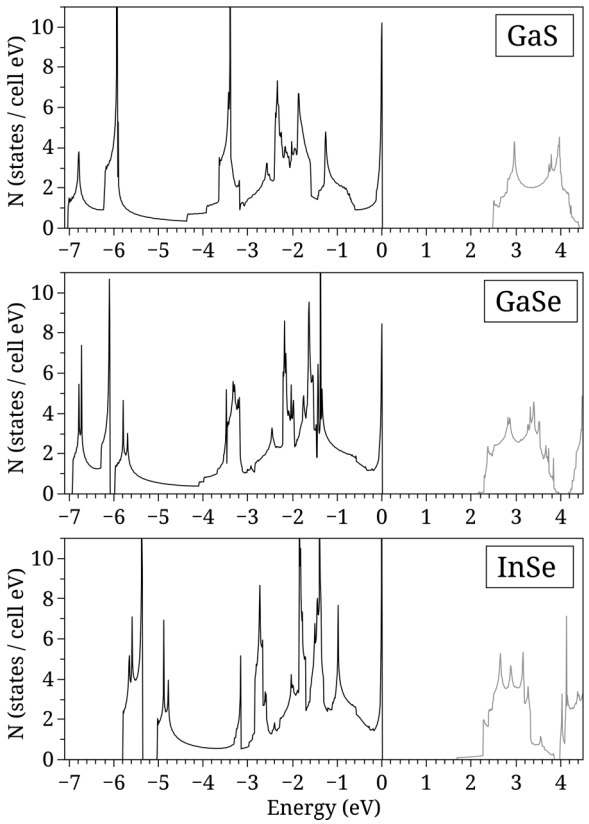

FIG. 4. The electronic density of states for single tetralayers of GaS, GaSe, and InSe, calculated from LDA band structures. A sharp peak at the top of the valence band originates from the ring-shaped band extremum.

Since we know that the macroscopic crystals of III-VI compounds have a parabolic valence band maximum (while the single tetralayers of these materials exhibit a qualitatively different, ring-shaped valence band maximum), it is interesting to find out at which thickness and how the transition between two types of extrema occurs.

B. Multi-tetralayer structures of GaS, GaSe, and InSe

To investigate the evolution of valence band shape of III-VI compounds with their thickness changing, we carried out the electronic structure computations for systems containing from 1 to 8 tetralayers stacked according to β-polytype. For each

TABLE II. The model dispersion parameters fitted to the numerical LDA bands in the round vicinity of Γ point with radius of 0.3 rad/bohr.

	GaS	GaSe	InSe
A	−0.0138	−0.0117	−0.0128
B	0.3080	0.3734	0.2965
C	0.0051	0.0105	0.0068
D	0.1211	0.1183	0.1044
E	0.0091	0.0089	0.0113

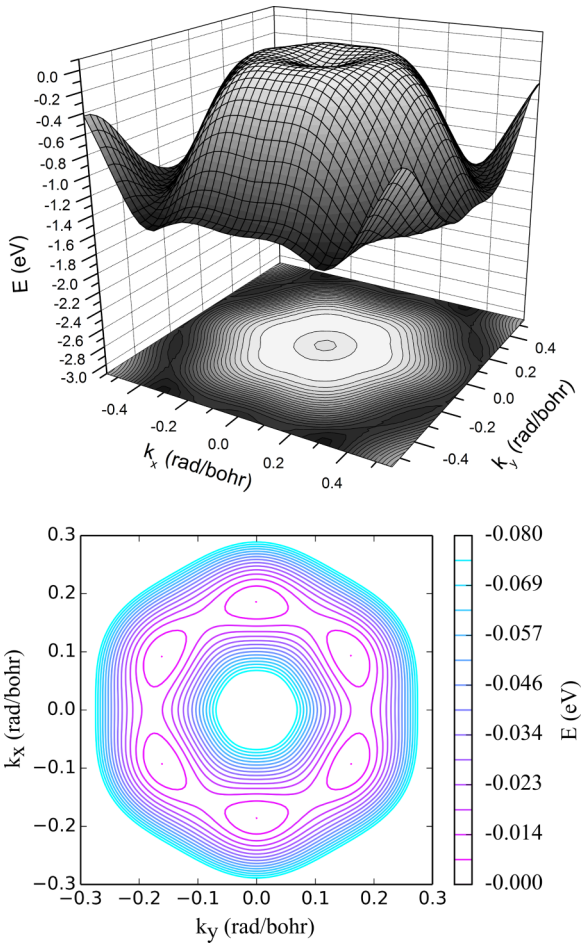

FIG. 5. (Color online) The topmost valence band surface of a single GaS tetralayer, calculated within the DFT in the vicinity of the first Brillouin zone, together with the corresponding contour plot (top) and the contour plot, obtained with use of the model dispersion 4 with parameters from Table II (bottom).

structure we performed a structural optimization for both the ion positions and the lattice constants.

An addition of new tetralayers to the system results in an appearance of new energy bands with their splitting due to interlayer interactions. Figure 6 shows the band structure fragments of 1, 2, and 3 GaS tetralayers along the Γ-K direction. The energy bands, formed by p_x and p_y orbitals of S atoms, undergo only small splitting due to a weak spatial overlap of adjacent tetralayer wave functions. p_z orbitals, in contrast, have an orientation perpendicular to the layer surface and interact strongly. This results in a strong splitting of corresponding energy bands. This affects the shape of the topmost valence band. As seen from Fig. 6, the maximum of the valence band shifts towards the Brilluin zone center with an increasing thickness, while the local minimum of dispersion at Γ is pushed out. Our calculations show that for β-GaS and β-GaSe the ring-shaped valence band maximum exists for thicknesses up to 5 and 7 tetralayers, respectively. This is, approximately, 3.9 nm and 5.6 nm (when taking the thickness of tetralayer as a half of the experimental value of c-lattice parameter). For β-InSe, our calculations revealed that

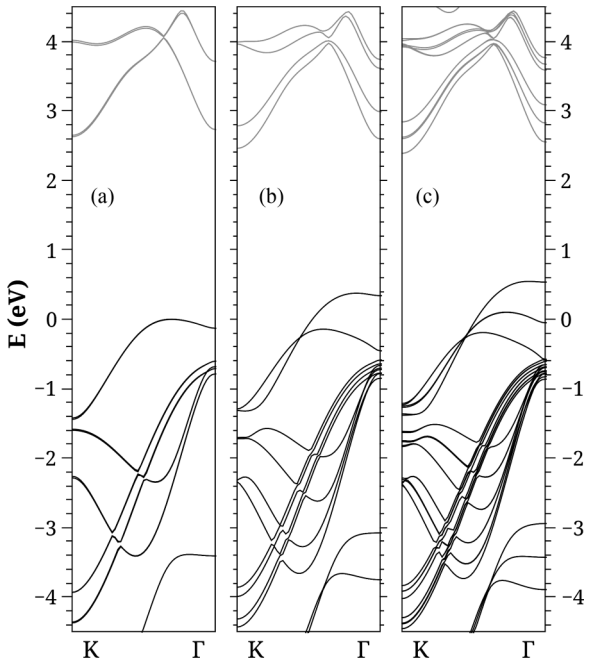

FIG. 6. The band structure fragments for one (a), two (b), and three (c) tetralayers of GaS. The energy curves containing Se p_z orbitals undergo the strongest splittings.

RSVB holds for up to 8 tetralayers—the maximal thickness we calculated by using the supercell approach. Computations of systems containing more than 8 layers are facing technical difficulties due to the limitations of computational resources.

To estimate the further behavior of band shape, we employ a simplified approach [sometimes referred to as the zone-folding method (ZFM)]. The ZFM can be used to calculate the band structure of a nanomaterial from the energy bands of the bulk crystal by application of boundary conditions on the electron wave vector. In our case the size-induced confinement is present in the z direction, and we have to determine a set of allowed k_z values from geometrical means, that is, the thickness of our structures. In this form the ZFM has been successfully applied to study the effect of confinement on the electronic structure of few-layer graphene [44]. The authors derived the following expression for k_z:

$$k_z = \frac{2\pi n}{(N+1)c}, \tag{5}$$

where c is a lattice parameter and N is the number of tetralayers, $n = \pm 1, \pm 2, \pm 3, \ldots, \pm\text{int}[(N+1)]$. Since we are interested only in the highest valence curves, we take $n = 1$. The resulting dispersions of the topmost valence bands for GaS, GaSe, and InSe obtained within the supercell approach, as well as some of the lines calculated with the ZFM, are shown in Fig. 7. The zero energy is counted from the bulk valence band maximum, while the energies of systems containing different numbers of tetralayers are aligned to one of the low-lying Ga/In $3d$ bands, that is almost unaffected by interlayer splitting. With increasing thickness, the radius of the ring-shaped extremum becomes smaller, and the local minimum at Γ is pushed out, until, at some critical thickness, a transition from RSVB

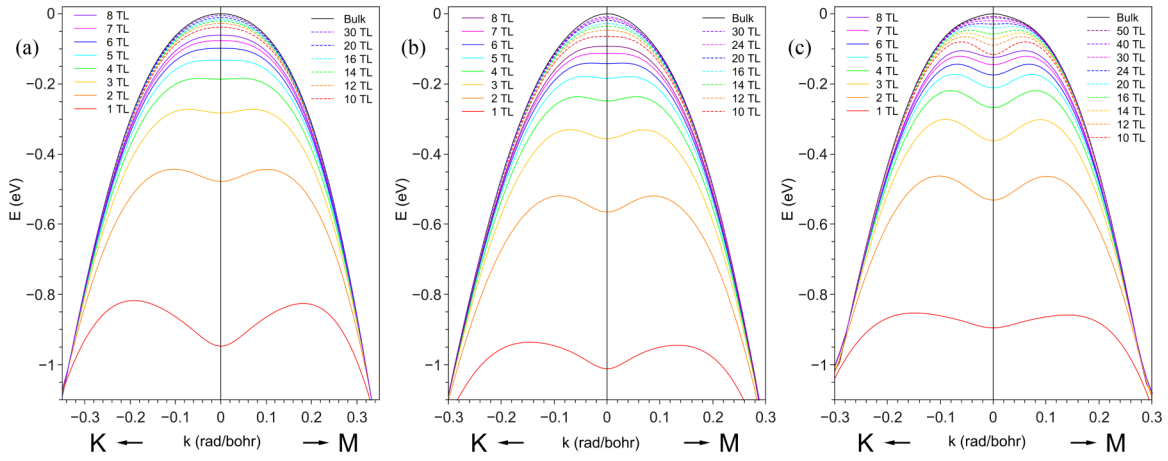

FIG. 7. (Color online) The evolution of the topmost valence band of β-GaS (a), β-GaSe (b), and β-InSe (c) with an increasing thickness. The solid lines correspond to results obtained within the supercell calculations, while the dotted lines are estimations from the zone-folding method.

to a parabolic band appears. At this critical thickness, the dispersion in the vicinity of the Γ point becomes almost flat. Above that thickness the topmost valence band exhibits the usual parabolic behavior. For β-GaS and β-GaSe the value of critical thickness was calculated to be equal to 6 and 8 tetralayers or ∼4.6 nm and ∼6.4 nm, respectively. ZFM estimation for β-InSe is 28 tetralayers (∼24.0 nm). Due to the deviations of ZFM results from those of a direct calculation, we would refer to the values of the critical thickness obtained in frames of ZFM as to the upper limits of true values.

The origin of transition between two different types of extremum can be understood on the basis of a $\boldsymbol{k}$-dependent orbital composition of the topmost valence band. As we already stated, the band splitting is stronger for the states containing p_z orbitals of S/Se atoms, which have a significant overlap in the interlayer space. In the case of the uppermost valence band, the amount of p_z component is maximal at the Γ point. The admixture of other types of orbitals occurs in the course of moving towards the Brillouin zone boundary. These new orbitals replace p_z-like wave functions, and the band splitting becomes smaller for $\boldsymbol{k}$ points far away from the zone center. To illustrate this idea we projected the wave functions of the topmost valence band on the atomic orbitals of atoms in a unit cell. In this basis the wave function at a given $\boldsymbol{k}$ point can be viewed as

$$\Psi_{\mathbf{k}}(\mathbf{r}) = \sum_{i,j} C_{i,j,\mathbf{k}} \chi_{i,\mathbf{k}}(\mathbf{r} - \mathbf{R}_{\mathbf{j}}), \tag{6}$$

where $\chi_{i,\mathbf{k}}$ $(\mathbf{r}-\mathbf{R}_j)$ is an atomic orbital of type i, centered on atom j, located at $\boldsymbol{R}_j$. $C_{i,j,\mathbf{k}}$ are the expansion coefficients, the squared modulus of which show the portion of corresponding orbital at point $\boldsymbol{k}$ in the wave function. The coefficients are normalized as following:

$$\sum_{i,j} |C_{i,j,\mathbf{k}}|^2 = 1, \tag{7}$$

though we encountered minor deviations from this relation during the numerical decomposition.

The dependence of these coefficients on $\boldsymbol{k}$ for a single GaSe tetralayer, together with the plot of the topmost valence band, omitting the SOC effects, is shown in Fig. 8. Since there are two atoms of each kind in the unit cell, we plot the magnitude of $2|C_{i,j}|^2$. From Fig. 8 it can be seen that the amount of Se p_z component is indeed the largest at the Γ point. The admixture of other orbitals, predominantly Ga p_z and Se p_x and p_y, occurs when moving towards the zone boundary. As a consequence, the strongest interlayer interaction of the topmost valence band occurs at Γ, and the local minimum of the dispersion is pushed out with an addition of new tetralayers.

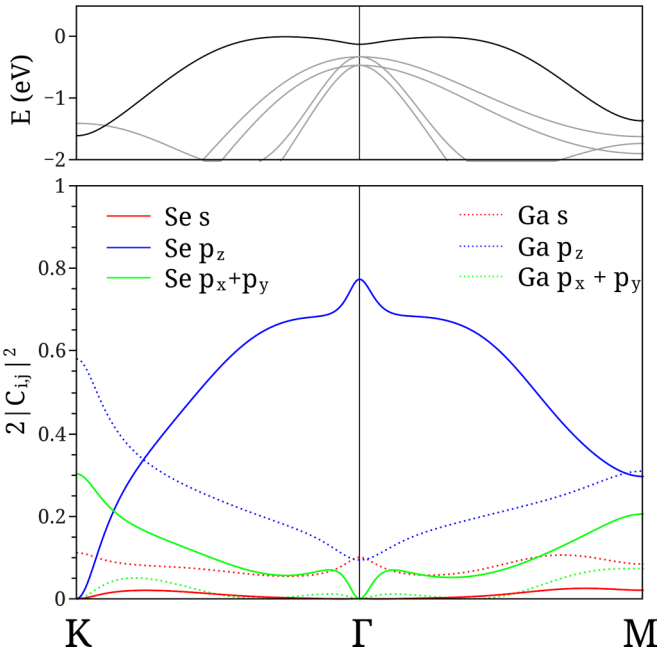

FIG. 8. (Color online) The topmost valence band of the single GaSe tetralayer (top) and its orbital composition (bottom) along the high-symmetry lines of the hexagonal Brillouin zone without SOC effects.

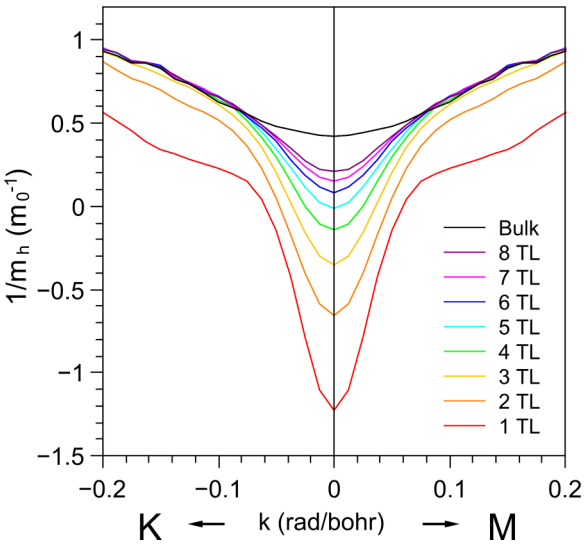

FIG. 9. (Color online) The dependence of the inverse hole mass on the wave vector for β-GaS. For few-layer structures, the effective mass is strongly $\boldsymbol{k}$ dependent.

C. Hole effective masses

Obviously, such strong changes in the valence band shape should be reflected in the magnitude of the hole effective masses. To study the hole masses, we took the second derivative of the numerical LDA energy bands. We found that for thin systems with few tetralayers, the hole effective masses become strongly $\boldsymbol{k}$ dependent (as can be seen from Fig. 9). The dependence of hole masses on tetralayer number for GaS, GaSe, and InSe of β polytype, calculated using the supercell (SC) and zone-folding methods (ZFM), is shown in Fig. 10. At the thickness below critical, the zone-center hole masses are negative due to an upwards curvature of valence band and are almost isotropic. The masses at the global maximum at $\boldsymbol{k}_{\max}$ are positive and highly anisotropic. When approaching the critical thickness, the local minimum at Γ becomes pushed out and the energy band in the vicinity of zone center becomes almost flat, leading to large hole masses in a small area of $\boldsymbol{k}$ space near Γ. At this thickness, the transition to the parabolic valence band occurs. A further increase of thickness leads to the increase of band curvature with the hole masses decreasing down to their bulk values. Figure 10 reveals some deviations of the results obtained with different methods. From the general tendencies we can conclude that the ZFM estimates the upper bound for critical thickness value. At the same time, both approaches confirm the existence of a transition from the ring-shaped to parabolic valence band while the thickness increases. We would also like to mention that our results hold for β modification of III-VI materials, while the values of critical thickness and effective masses may differ for other polytypes.

We should also discuss the possible influence of the underestimation of the band gap, common for LDA calculations, on the values of the effective masses. As we have shown, the zone-center hole masses in GaS, GaSe, and InSe are mostly affected by the interaction with underlying valence bands. The interaction with the higher conduction band is small, and this leads to a fair reproduction of the hole masses even in the presence of an underestimated band gap. For example, the calculated in-plane hole mass for β-GaSe ($1.0m_0$) is in fair agreement with the available experimental data ($0.8m_0$). At the same time, the value of the band gap affects the zone center masses of the conduction band electrons, since their magnitude is determined by the interaction with the valence band Γ_3^-. Therefore, to study the behavior of the electron masses, one has to employ methods capable of the correct estimation of the band gap.

These findings show that the hole effective masses in III-VI layer compounds depend strongly on the thickness, and this might open a way for a size-controlled engineering of charge carrier properties. Another important question is the behavior of hole masses at the critical thickness, where the valence band is almost flat in a small region of $\boldsymbol{k}$ space. Since there are no experimental results on the hole masses for thin III-VI crystals, we will try to draw an analogy with a similar effect, appearing in bulk InSe under pressure. In this case, the authors also predicted from first principles the occurrence of singularity at some pressure, but the experiments did not reveal any signs of this feature [35]. The authors explained this discrepancy by a possible appearance of a substitutional valence band maximum due to the spin-orbit coupling effects, which were absent in their calculations. In our case, SOC was taken into account, but no additional maximums at the topmost valence band have been revealed. Therefore, the behavior of the III-VI

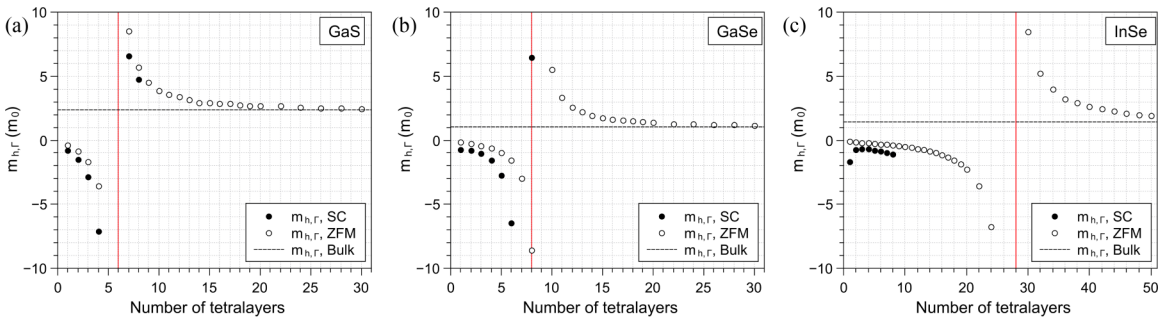

FIG. 10. (Color online) The dependence of zone-center hole effective masses of β-GaS (a), β-GaSe (b), and β-InSe (c) on the number of tetralayers, calculated with the supercell (SC, full circles) approach and the zone-folding method (ZFM, open circles). The dotted horizontal line depicts the calculated value of bulk material. The red vertical line shows the critical thickness of structures, where the transition from the ring-shaped valence band to the parabolic band occurs.

layer material electronic structure at their critical thickness, where the transition between two types of band extrema occur, may be an object for further study, both theoretical and experimental.

IV. CONCLUSIONS

In summary, in this paper we present the results of first-principles electronic structure calculations of the valence band structures of few-layer GaS, GaSe, and InSe. We investigate the dependence of the band shape on the crystal thickness and show the presence of a transition between two types of band extrema at some critical thickness. The value of this thickness was calculated to be equal to 6 tetralayers (∼4.6 nm) and 8 tetralayers (∼6.4 nm) for β-GaS and β-GaSe and was estimated to be below 28 tetralayers (∼24.0 nm) for β-InSe, respectively. The existence of ring-shaped extrema in few-layer GaS, GaSe, and InSe can be understood on the basis of $\boldsymbol{k}\cdot\boldsymbol{p}$ theory linking the curvature of energy bands and the distance between them. The transition from RSVB to the parabolic valence band occurs due to a $\boldsymbol{k}$-dependent orbital composition of the topmost valence band, which leads to a strong interaction of the bands in the Brillouin zone center, while only a weak interaction at the zone boundary. The hole effective masses have been found to be $\boldsymbol{k}$ dependent in the few-layer systems and were shown to depend strongly on the number of tetralayers in the vicinity of critical thickness. We have therefore proposed a way of controlling the charge carrier properties in III-VI systems by tuning their thickness.

ACKNOWLEDGMENTS

This work was supported by the SP-7452.2013.5 and RFBR 14-32-50852 mol_nr projects and RAS research programs.

[1] A. Brukl and G. Ortner, Naturwiss. **18**, 393 (1930).
[2] W. C. Johnson and B. Warren, Naturwiss. **18**, 666 (1930).
[3] W. Klemm and H. U. v. Vogel, Z. Anorg. Allg. Chem. **219**, 45 (1934).
[4] H. Hahn, Angew. Chem. **65**, 538 (1953).
[5] K. Schubert and E. Dörre, Naturwiss. **40**, 604 (1953).
[6] K. Schubert and E. Dörre, Naturwiss. **41**, 448 (1954).
[7] K. Schubert, E. Döre, and M. Kluge, Z. Metallkunde **46**, 216 (1955).
[8] S. A. Semiletov, Sov. Phys. Cryst. **3**, 288 (1958).
[9] G. A. Akhundov, A. A. Agaeva, V. M. Salmanov, Y. P. Sharonov, and I. D. Yaroshetskii, Sov. Phys. Semicond. **7**, 826 (1973).
[10] V. I. Sokolov, Y. F. Solomonov, and V. K. Sobashiev, Sov. Phys. Solid State **17**, 1256 (1976).
[11] I. M. Catalano, A. Cingolani, A. Minafra, and C. Paorici, Opt. Commun. **24**, 105 (1978).
[12] Y. F. Solomonov and V. K. Sobashiev, Phys. Status Solidi A **74**, 75 (1982).
[13] G. B. Abdullaev, K. R. Allakverdiev, M. E. Karaseev, V. I. Konov, L. A. Kulewskii, N. B. Mustafaev, P. P. Pashinin, A. M. Prokhorov, Y. M. Starodunov, and N. I. Chapliev, Sov. J. Quantum Electron. **19**, 494 (1989).
[14] E. Bringuier, A. Bourdon, N. Piccioli, and A. Chevy, Phys. Rev. B **49**, 16971 (1994).
[15] K. L. Vodopyanov, L. A. Kulevskii, V. G. Voevodin, A. I. Gribenyukov, K. R. Allakhverdiev, and T. A. Kerimov, Opt. Commun. **83**, 322 (1991).
[16] A. Bianchi, A. Ferrario, and M. Musci, Opt. Commun. **25**, 256 (1978).
[17] J. L. Oudar, P. J. Kupecek, and D. S. Chemla, Opt. Commun. **29**, 119 (1979).
[18] P. J. Kupecek, H. L. Person, and M. Comte, Infrared Phys. **19**, 263 (1979).
[19] M. Schlüter, Nuovo Cimento B **13**, 313 (1973).
[20] A. Kuhn, A. Chevy, and R. Chevalier, Phys. Status Solidi A **31**, 469 (1975).
[21] F. Jellinek and H. Hahn, Z. Naturforsch. B **16**, 713 (1961).
[22] K. S. Novoselov, A. K. Geim, S. V. Morozov, D. Jiang, Y. Zhang, S. V. Dubonos, I. V. Grigorieva, and A. A. Firsov, Science **306**, 666 (2004).
[23] D. J. Late, B. Liu, H. S. S. R. Matte, C. N. R. Rao, and V. P. Dravid, Adv. Funct. Mater. **22**, 1894 (2012).
[24] P. Hu, Z. Wen, L. Wang, P. Tan, and K. Xiao, ACS Nano **6**, 5988 (2012).
[25] G. Fisher, Helv. Phys. Acta **36**, 317 (1963).
[26] F. Bassani and G. P. Parravicini, Nuovo Cimento B **50**, 95 (1967).
[27] H. Kamimura and K. Nakao, J. Phys. Soc. Jpn. **24**, 1313 (1968).
[28] J. V. McCanny and R. B. Murray, J. Phys. C **10**, 1211 (1977).
[29] V. K. Bashenov, D. I. Marvakov, and A. G. Petukhov, Phys. Status Solidi B **90**, K5 (1978).
[30] J. Robertson, J. Phys. C **12**, 4777 (1979).
[31] D. V. Rybkovskiy, N. R. Arutyunyan, A. S. Orekhov, I. A. Gromchenko, I. V. Vorobiev, A. V. Osadchy, E. Y. Salaev, T. K. Baykara, K. R. Allakhverdiev, and E. D. Obraztsova, Phys. Rev. B **84**, 085314 (2011).
[32] D. V. Rybkovskiy, I. V. Vorobyev, A. V. Osadchy, and E. D. Obraztsova, J. Nanoelectron. Optoelectron. **7**, 65 (2012).
[33] V. Zólyomi, N. D. Drummond, and V. I. Fal'ko, Phys. Rev. B **87**, 195403 (2013).
[34] A. Segura, F. J. Manjón, D. Errandonea, J. Pellicer-Porres, V. Muñoz, G. Tobias, P. Ordejón, E. Canadell, A. S. Miguel, and D. Sánchez-Portal, Phys. Status Solidi B **235**, 267 (2003).
[35] D. Errandonea, A. Segura, F. J. Manjón, A. Chevy, E. Machado, G. Tobias, P. Ordejón, and E. Canadell, Phys. Rev. B **71**, 125206 (2005).
[36] A. Segura, D. Errandonea, D. Martínez-García, F. J. Manjón, A. Chevy, G. Tobias, P. Ordejón, and E. Canadell, Phys. Status Solidi B **244**, 162 (2007).
[37] J. P. Perdew, K. Burke, and M. Ernzerhof, Phys. Rev. Lett. **77**, 3865 (1996).
[38] J. P. Perdew, A. Ruzsinszky, G. I. Csonka, O. A. Vydrov, G. E. Scuseria, L. A. Constantin, X. Zhou, and K. Burke, Phys. Rev. Lett. **100**, 136406 (2008).
[39] S. Grimme, J. Comput. Chem. **27**, 1787 (2006).
[40] V. Barone, M. Casarin, D. Forrer, M. Pavone, M. Sambi, and A. Vittadini, J. Comput. Chem. **30**, 934 (2008).
[41] A. Kuhn, A. Chevy, and R. Chevalier, Acta Cryst. B **32**, 983 (1976).
[42] A. Likforman, D. Carre, J. Etienne, and B. Bachet, Acta Cryst. B **31**, 1252 (1975).

[43] P. Giannozzi, S. Baroni, N. Bonini, M. Calandra, R. Car, C. Cavazzoni, D. Ceresoli, G. L. Chiarotti, M. Cococcioni, I. Dabo, A. Dal Corso, S. de Gironcoli, S. Fabris, G. Fratesi, R. Gebauer, U. Gerstmann, C. Gougoussis, A. Kokalj, M. Lazzeri, L. Martin-Samos, N. Marzari, F. Mauri, R. Mazzarello, S. Paolini, A. Pasquarello, L. Paulatto, C. Sbraccia, S. Scandolo, G. Sclauzero, A. P. Seitsonen, A. Smogunov, P. Umari, and R. M. Wentzcovitch, J. Phys. Condens. Matter **21**, 395502 (2009).

[44] K. F. Mak, M. Y. Sfeir, J. A. Misewich, and T. F. Heinza, Proc. Natl. Acad. Sci. USA **107**, 14999 (2010).